ORIGINAL ARTICLE



Impact of asymmetricity of indexable cutter bodies on chatter resistance

Hatice Elif Tola Demirel¹ · Bekir Bediz² · Jokin Munoa³ · Zekai Murat Kilic¹

Received: 25 January 2025 / Accepted: 13 August 2025 © The Author(s) 2025

Abstract

Milling operations are often limited by regenerative chatter vibrations arising due to the flexible machine tool parts which have dynamic effects on both stationary and rotary directions. Additionally, asymmetricity (or, non-axisymmetricity) of the milling cutter has an impact on rotating dynamics of the machine tool. However, asymmetric cutters may not always have positive effects; hence, care must be taken when using them. This paper investigates how to achieve desired chatter stability characteristics by tuning the dynamic response of the tool body. Both frequency and time domain methods were used to predict the stability lobes diagram according to the measured tool tip frequency response functions. An indexable end mill with exchangeable head (namely, tool bit) is used for demonstration of dynamic tuning. Additionally, receptance coupling substructure analysis is used to predict the tool tip frequency response function for various degrees of asymmetry. The down milling cutting tests validated that the proposed approach captures the sensitivity of the stability lobes diagram to the degree of asymmetricity.

Keyword Chatter stability · Non-axisymmetric cutter · Rotating dynamics

1 Introduction

Regenerative vibration is the main mechanism of chatter (or, self-excited vibrations) that limits productivity in milling operations. An established method to avoid chatter for a machining operation in the industry is to use stability lobes diagram (SLD) that predicts chatter-free cutting conditions for safe and accurate machining with more productivity. Altintas et al. [1] explain the evolution of SLD prediction with the advancements in machining process modeling since the pioneering works of Tobias and Fishwick [2] and Tlusty and Polacek [3]. Currently, two solution methods are widely accepted as benchmarks for SLD predictions in milling operations. The first one is the frequency domain approach by Altintas and Budak [4]; they proposed the zero order

analytical (ZOA) method to directly solve the eigenvalues for critical depth of cut and chatter frequency in milling by averaging the time-varying periodic directional coefficients matrix. The second one is the time domain approach by Insperger and Stepan [5]; they proposed the semi-discretization (SD) method that solves the time-varying chatter stability problem by evaluating the stability of the periodic state transition matrix based on Floquet's theory.

If SLD cannot provide acceptable productivity, there are ways to modify the system externally through active and passive methods and modify the SLD by disturbing the chatter mechanism [6]. Compared to active damping methods which require additional power, passive methods are easier to implement as they modify the machine tool or workpiece. Among the passive methods, tool geometry modification is commonly applied to improve machining stability [7], with many applications in the industry such as the variable pitchvariable helix cutters. However, such tools may be more expensive to produce and may not show expected outcomes as their geometry should be ideally designed according to the machine tool's dynamics. For tools with long cutter bodies, implementing the tuned-mass-damper concept is another effective solution, but they may also need tunable natural frequency [8]. Considering that tool modification may depend

Published online: 13 September 2025

- School of Engineering, The University of Manchester, Oxford Rd, Manchester, UK
- Faculty of Engineering and Natural Sciences, Sabanci University, Istanbul, Turkey
- ³ Ideko, Dynamics and Control, Elgoibar, Basque Country, Spain



on dynamic response of the machine tool, recent studies also focused on tuning the tool body's frequency response function (FRF). As a result, vibrations were suppressed quite effectively by mode coupling between the spindle holder and tool [9–11]. Although a simple yet effective solution would be to use a cutter body with asymmetric geometry, not much attention was shown to the design of such cutters.

A typical SLD prediction for milling uses non-rotating frames, i.e., both tool and workpiece coordinate frames are presumed to be fixed or non-rotating. However, since the tool is rotational in milling, a rotating frame may be needed to capture the gyroscopic effects for the cutters with nonaxisymmetric or asymmetric dynamics. During rotation, the tool vibration would be split into two modes, namely forward and backward modes, which would have increased differences in natural frequencies at higher spindle speeds [12]. Bediz et al. experimentally investigated the speed-dependent dynamics of a spindle by using a custom-made impact excitation system [13]. In another study, Cheng et al. identified the dynamics at the tool tip by impact testing of a rotating cylindrical standard artifact [14]. Both studies show that the dynamics of the system are indeed affected due to the gyroscopic effects at high rotational spindle speeds. Previously, for boring operations, Li et al. [15] showed that the rotating dynamics of the flexible boring tool have significant effects on the chatter stability. Eynian and Altintas [16] proposed a method for predicting chatter stability for milling a flexible workpiece with an asymmetric end mill including its rotating dynamics and process damping effects. Then, Comak et al. [17] solved milling stability with an asymmetric cutter including rotating dynamics in both frequency and discrete time domain and experimentally validated the method for a two-fluted end mill. Since single and two-fluted end mills can be asymmetric due to non-symmetric flute geometry, their case with a four-fluted end mill has symmetric dynamics. Previous studies mostly analyzed the existing non-symmetric dynamics of the asymmetric tools and did not explore the potential of using asymmetricity to improve stability. Recently, Baumann et al. [18] converted a symmetric end milling into an asymmetric one by machining flat surfaces along its shank. They investigated the improvements by experiment trials and discussed the positive benefits of cutter's asymmetric geometry on the chatter stability. However, as asymmetricity adds gyroscopic effects, the interaction between the resulting forward and backward modes may not always improve the stability. Therefore, further investigations based on mathematical modeling of the milling process are required to show such effects.

This paper investigates the effects of the rotating dynamics of a four-fluted asymmetric end mill on the chatter stability of milling operations. Previously, four-fluted end mills and indexable cutters were not studied for asymmetric tools. Moreover, there was no model-based investigation to

improve the stability using the asymmetricity of the tools. For the first time, this study shows that asymmetric tools may not always increase stability. By using a variation of the frequency domain solutions of Eynian and Altintas [16] and Comak et al. [17], which is verified by experiments and time domain simulations, SLDs of indexable cutters with axisymmetric and non-axisymmetric cutter bodies are simulated and compared to show the impact on stable cutting conditions. While the gyroscopic effects related to asymmetricity of the cutter shank are considered, the effects of the spindle speed on modal parameters are not within the scope of the paper. However, the method can be extended to include speed dependent dynamics which can be measured by a dedicated experimental setup. Additionally, the receptance coupling substructure analysis (RCSA) is employed to identify the joint stiffness characteristics based on the symmetric cutter's measured response, and then to predict the tool tip FRF of the cutter bodies with various degrees of asymmetricity. The findings were supported by experimental validation.

2 Chatter prediction with asymmetric dynamics

This section presents the formulation for a cutter with rotating vibration modes, following the steps presented in [16, 17].

2.1 Dynamic equation of the rotating tool

A schematic representation of end milling process is shown in Fig. 1. Here, xy represents the fixed (non-rotating) coordinate frame, while uv is the rotating frame. The dynamics of the milling operation can be described in the fixed coordinates (x, y) by the following equation:

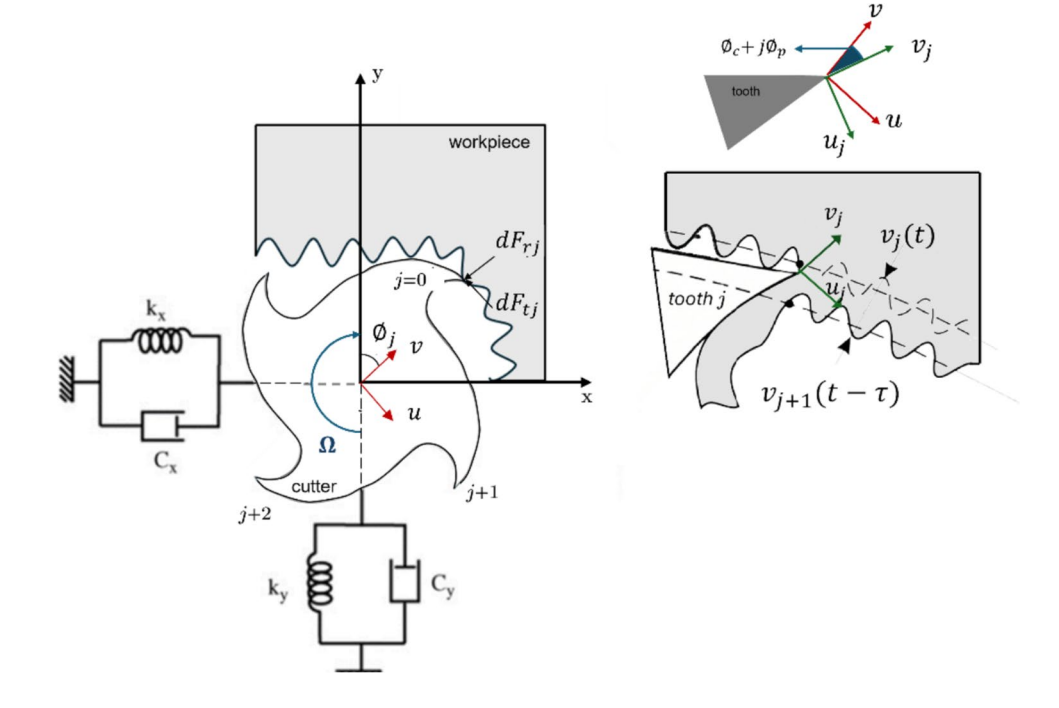
$$\left\{ \begin{array}{l} \boldsymbol{F}_{x}(t) \\ \boldsymbol{F}_{y}(t) \end{array} \right\} = \left[\boldsymbol{M}_{xy} \right] \left\{ \begin{array}{l} \ddot{\boldsymbol{x}} \\ \ddot{\boldsymbol{y}} \end{array} \right\} + \left[\boldsymbol{C}_{xy} \right] \left\{ \begin{array}{l} \dot{\boldsymbol{x}} \\ \dot{\boldsymbol{y}} \end{array} \right\} + \left[\boldsymbol{K}_{xy} \right] \left\{ \begin{array}{l} \boldsymbol{x}(t) \\ \boldsymbol{y}(t) \end{array} \right\}$$
 (1)

where the mass (M_{xy}) , the damping (C_{xy}) and the stiffness (K_{xy}) matrices are constant, and the displacement and force vectors, $\{x(t)\ y(t)\}^T$ and $\{F_x(t)\ F_y(t)\}^T$ are in the fixed coordinates.

Tool tip frequency response function (FRF) is affected by the dynamics of the non-symmetrical parts of the cutter body while the tool rotates. Therefore, writing the equation of motion by including the rotating vibration modes would represent the process dynamics more accurately. Vibration displacement vector $\{x(t) y(t)\}^T$ in the fixed coordinate frame can be related to the displacement vector $\{u(t) v(t)\}^T$ in the rotating coordinate frame by the orthonormal transformation matrix as follows: [16]



Fig. 1 Dynamics of the cutter in rotating coordinates frame (u, v)



$$\begin{cases} x(t) \\ y(t) \end{cases} = T(t) \begin{cases} u(t) \\ v(t) \end{cases}; \qquad T(t) = \begin{bmatrix} \cos(\phi) & \sin(\phi) \\ -\sin(\phi) & \cos(\phi) \end{bmatrix}; \qquad \phi(t) = \Omega t \qquad \qquad T^{-1}T \begin{cases} F_u \\ F_v \end{cases} = T^{-1}M_{xy}T \begin{cases} \ddot{u} \\ \ddot{v} \end{cases} + T^{-1} \left(2M_{xy}\dot{T} + C_{xy}T\right) \begin{cases} \dot{u} \\ \dot{v} \end{cases} + T^{-1} \left(2M_{xy}\dot{T} + C_{xy}T\right) \begin{cases} \dot{u} \\ \dot{v} \end{cases} \end{cases} + T^{-1} \left(2M_{xy}\dot{T} + C_{xy}T\right) \begin{cases} \dot{u} \\ \dot{v} \end{cases}$$

where T(t) is the rotation matrix to represent rotating coordinates (u, v) in fixed frame (x, y), $\phi(t)$ is the angular location of the tool's reference tooth (at j = 1, i.e., $\phi = \phi_1$ in Fig. 1) in rad, Ω is the spindle speed in rad/s and t is time in s. Taking the first and second derivatives of the displacement vector $\{x(t) \ y(t)\}^T$ in Eq. (3), velocity and acceleration vectors in the rotating coordinate frame (u, v)can be expressed as follows:

Similarly in Eq. (4), the force vector can be transformed from fixed into rotating coordinates as

Substituting Eqs. (3) and (4) into Eq. (1) yields

$$T \begin{cases} F_{u} \\ F_{v} \end{cases} = M_{xy}T \begin{cases} \dot{u} \\ \ddot{v} \end{cases} + \left(2M_{xy}\dot{T} + C_{xy}T\right) \begin{cases} \dot{u} \\ \dot{v} \end{cases} + \left(M_{xy}\ddot{T} + C_{xy}\dot{T} + K_{xy}T\right) \begin{cases} u \\ v \end{cases}$$
(5)

Multiplying each side by T^{-1} gives the equation of motion in rotating coordinates:

$$T^{-1}T \begin{Bmatrix} F_{u} \\ F_{v} \end{Bmatrix} = T^{-1}M_{xy}T \begin{Bmatrix} \ddot{u} \\ \ddot{v} \end{Bmatrix} + T^{-1} \left(2M_{xy}\dot{T} + C_{xy}T \right) \begin{Bmatrix} \dot{u} \\ \dot{v} \end{Bmatrix} + T^{-1}$$

$$\left(M_{xy}\ddot{T} + C_{xy}\dot{T} + K_{xy}T \right) \begin{Bmatrix} u \\ v \end{Bmatrix}$$

$$(6)$$

where M_{uv} , C_{uv} and K_{uv} are constant mass, damping and stiffness matrices in rotating coordinate frame. Presuming a single vibration mode in each coordinate axis u and v, they can be written as follows:

$$\mathbf{M}_{uv} = \begin{bmatrix} m_u & 0 \\ 0 & m_v \end{bmatrix}; \qquad \mathbf{C}_{uv} = \begin{bmatrix} c_u & 0 \\ 0 & c_v \end{bmatrix}; \qquad \mathbf{K}_{uv} = \begin{bmatrix} k_u & 0 \\ 0 & k_v \end{bmatrix}, \tag{8}$$

with the modal mass m_u and m_v , damping c_u and c_v and stiffness k_u and k_v . C_{cor} in Eq. (8) is due to the Coriolis forces, while K_{crc} and K_{cnt} are the centripetal and circulatory terms; they all depend on spindle speed Ω and are defined as follows:

$$C_{cor} = 2\Omega \begin{bmatrix} 0 & m_u \\ -m_v & 0 \end{bmatrix} \qquad K_{cnt} = \Omega^2 \begin{bmatrix} -m_u & 0 \\ 0 & -m_v \end{bmatrix} \qquad K_{crc} = \Omega \begin{bmatrix} 0 & c_u \\ -c_v & 0 \end{bmatrix}$$
(9)

2.2 Model of the dynamic cutting forces

In Fig. 1, the chip thickness $h_i(t)$ removed by j-th cutting edge depends on the vibration in the local normal



direction (v) of current and previous cutting edges, i.e., $h_j(t) = h_0(t) + v_j(t) - v_{j+1}(t-T)$ with static chip thickness $h_0(t)$ and tooth passing period T as the delay term. Thus, dropping the static chip thickness term as it does not contribute to the dynamic loading, the following can be written in local coordinates (u_i, v_j) : [17]

$$h_{j}(t) = \begin{bmatrix} 0 & 1 \end{bmatrix} \left\{ \begin{array}{l} u_{j}(t) - u_{j+1}(t-\tau) \\ v_{j}(t) - v_{j+1}(t-\tau) \end{array} \right\}$$
 (10)

where $\{u_j(t) \ v_j(t)\}^T$ and $\{u_{j+1}(t-T) \ v_{j+1}(t-T)\}^T$ are the current and delayed vibration vectors.

Dynamic forces in tangential and radial directions can be used to get the force vector in local coordinates as

$$\boldsymbol{F}_{t,j} = -g(\phi_j)aK_{tc}h_j(t); \quad \boldsymbol{F}_{r,j} = -g(\phi_j)aK_{rc}\boldsymbol{h}_j(t) = K_r\boldsymbol{F}_{t,j}$$
(11)

$$\left\{ \begin{array}{c} F_{u,j} \\ F_{v,j} \end{array} \right\} = - \left\{ \begin{array}{c} F_{t,j} \\ F_{r,j} \end{array} \right\} = - g\left(\phi_{j}\right) a K_{tc} \left(\begin{array}{c} 1 \\ K_{r} \end{array} \right) \left[\begin{array}{c} 0 \end{array} 1 \right] \left\{ \begin{array}{c} u_{j}(t) - u_{j+1}(t-\tau) \\ v_{j}(t) - v_{j+1}(t-\tau) \end{array} \right\}$$
 (12)

where K_{tc} and K_{rc} are cutting coefficients at the tangential and radial directions with K_r being their ratio ($K_r = K_{rc}/K_{tc}$), is the axial depth of cut, ϕ_j is the immersion angle of j-th tooth and $g(\phi_j)$ is the unit step function that can be expressed as

$$g(\phi_j) = \begin{cases} 1, & \phi_{st} - (j-1)\phi_p - \phi_c \le mod(\phi, 2\pi) \le \phi_{ex} - (j-1)\phi_p - \phi_c \\ 0, & otherwise \end{cases}$$
 (13)

where ϕ_{st} and ϕ_{ex} are the entry and exit angles of the cutter, pitch angle is $\phi_p = 2\pi/N$ for *N*-tooth cutter and ϕ_c is the offset angle between the local coordinate frame of the reference tooth $(u_{j=1}, v_{j=1})$ and the principal coordinate frame (u, v), as is shown in Fig. 1.

Displacements in the principal rotating coordinate frame (u, v) can be represented in the local rotating coordinate frame (u_j, v_j) by introducing the orthonormal rotation matrix that can be written as [17]

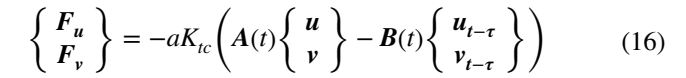
$$\begin{cases} u_{j}(t) \\ v_{j}(t) \end{cases} = R_{j} \begin{cases} u(t) \\ v(t) \end{cases} \qquad R_{j} = \begin{bmatrix} \cos\left((j-1)\phi_{p} + \phi_{c}\right) & -\sin\left((j-1)\phi_{p} + \phi_{c}\right) \\ \sin\left((j-1)\phi_{p} + \phi_{c}\right) & \cos\left((j-1)\phi_{p} + \phi_{c}\right) \end{bmatrix}$$

$$(14)$$

The total cutting forces in the principal coordinate frame (u, v) can be expressed as

$$\begin{Bmatrix} F_u \\ F_v \end{Bmatrix} = \sum_{j=1}^N \left[R_j \right]^{-1} \begin{Bmatrix} F_{uj} \\ F_{vj} \end{Bmatrix}$$
(15)

Substituting Eq. (12) into Eq. (15) and rearranging yields the cutting forces in principal coordinates as



where:

$$\mathbf{A}(t) = \sum_{j=1}^{N} g(\phi_j) \left[\mathbf{R}_j \right]^{-1} \begin{pmatrix} 1 \\ K_r \end{pmatrix} \left[0 \ 1 \right] \left[\mathbf{R}_j \right];$$

$$\mathbf{B}(t) = \sum_{j=1}^{N} g(\phi_j) \left[\mathbf{R}_j \right]^{-1} \begin{pmatrix} 1 \\ K_r \end{pmatrix} \left[0 \ 1 \right] \left[\mathbf{R}_{j+1} \right]$$
(17)

2.3 Zero-order analytical (ZOA) solution in frequency domain

For the equation of motion in fixed coordinate frame, Altintas and Budak [4] predicted the stability of vibrations by averaging the time-varying terms and solving the equation in the frequency domain. The same procedure is utilized in rotating coordinate frame [17]. The relation between displacements and forces can be described in the frequency domain with the tool tip frequency response matrix Φ_{uv} defined in rotating coordinate frame using Eq. (7):

$$\begin{cases}
 u(\omega) \\
 v(\omega)
\end{cases} = \Phi_{uv}(\omega) \begin{cases}
 F_{u}(\omega) \\
 F_{v}(\omega)
\end{cases}; \quad \Phi_{uv} \\
 = \left[-\omega^{2} M_{uv} + i\omega(C_{uv} + C_{cor}) + (K_{uv} + K_{crc} + K_{cnt}) \right]^{-1}$$
(18)

Using Eq. (18), Eq. (16) can be expressed in the frequency domain as follows:

$$\begin{cases}
F_{u}(\omega) \\
F_{v}(\omega)
\end{cases} = -aK_{tc} \left(A(\omega) - B(\omega)e^{-i\omega T} \right) \Phi_{uv}(\omega) \begin{cases}
F_{u}(\omega) \\
F_{v}(\omega)
\end{cases}$$
(19)

Since A(t) and B(t) matrices in Eq. (16) are periodic at tooth passing frequency, their Fourier series expansion form can be utilized in Eq. (19). Averaging them by recalling that R_j in Eq. (14) is constant yields

$$\overline{A} = \frac{\phi_{ex} - \phi_{st}}{2\pi} \sum_{j=1}^{N} [R_j]^{-1} \begin{pmatrix} 1 \\ K_r \end{pmatrix} \begin{bmatrix} 0 & 1 \end{bmatrix} [R_j]; \quad \overline{B} = \frac{1}{2\pi} \sum_{j=1}^{N} [R_j]^{-1} \begin{pmatrix} 1 \\ K_r \end{pmatrix} \begin{bmatrix} 0 & 1 \end{bmatrix} [R_{j+1}].$$
(20)

Presuming that $A(\omega) \sim \overline{A}$ and $B(\omega) \sim \overline{B}$, Eigenvalue equation is obtained by substituting Eq. (20) into Eq. (19):

$$\left\{ \begin{array}{l} \boldsymbol{F}_{u} \\ \boldsymbol{F}_{v} \end{array} \right\} = -aK_{tc} \left(\overline{\boldsymbol{A}} - \overline{\boldsymbol{B}} e^{-i\omega T} \right) \boldsymbol{\Phi}_{uv} \left\{ \begin{array}{l} \boldsymbol{F}_{u} \\ \boldsymbol{F}_{v} \end{array} \right\} \tag{21}$$

The characteristic equation can be written as

$$\det\left(\boldsymbol{I} + aK_{tc}\left(\overline{\boldsymbol{A}} - \overline{\boldsymbol{B}}e^{-i\omega T}\right)\boldsymbol{\Phi}_{uv}(\omega)\right) = \{0\}$$
 (22)



Stability lobes of the rotating milling system can be predicted by using the Nyquist stability criterion [19]. The eigenvalue problem is solved for each spindle speed, critical depth of cut and chatter frequency combinations.

2.4 Prediction of the tool tip frequency response function (FRF)

The costly and time-consuming measurements for each modified tool shape can be avoided by analytical prediction of the tool tip frequency response function (FRF) of the suggested cutter body geometry. As shown in Fig. 2, structural dynamic response at the holder–tool interface is identified to predict the tool tip FRF without producing the actual asymmetric cutter. After the identification of the holder tip FRF, the tool tip FRF can be predicted by forward receptance coupling substructure analysis (RCSA) of the cutter shank and the tool bit.

In this paper, first, the dynamics at the holder–cutter shank interface is identified by the inverse RCSA proposed by Park et al. [20] and Namazi et al. [21]. The translational FRFs of the coupled system $(HTS_{11}, HTS_{12}, \text{and } HTS_{22})$ are measured by three impact hammer tests. The mass effect

of the accelerometer is removed from all measurements by structural modification method proposed by Ozguven [22]. The symmetric cutter shank is assumed to be formed by Timoshenko beam segments. The both translational and rotational elements of the free-free symmetric cutter shank $(TS_{11}, TS_{12} \text{ and } TS_{22})$ receptance FRFs are analytically calculated, and by following the procedure in [21], the translational and rotational FRFs at the free end of the holder (H_{22}) are identified (Fig. 2a).

For the accurate prediction of the tool tip FRF, the contact parameters at the cutter shank—tool bit interface need to be identified. First, translational FRFs at the tool tip and at the interface of the cutter shank and the tool bit of the symmetric tool assembly ($HTSB_{11}$, $HTSB_{12}$ and $HTSB_{22}$) are measured by three impact hammer tests. Then, the FRF of the free-free tool bit that is assumed to be formed by Timoshenko beam segments is calculated. Again, following the inverse RCSA procedure in [21], dynamics at the cutter shank—tool bit interface ($HTS'_{11,i}$) is identified (Fig. 2b). By forward RCSA, the dynamics at the cutter shank—tool bit interface ($HTS'_{11,p}$) is predicted by including the tool bit part inside the cutter shank. The contact parameters at the interface are

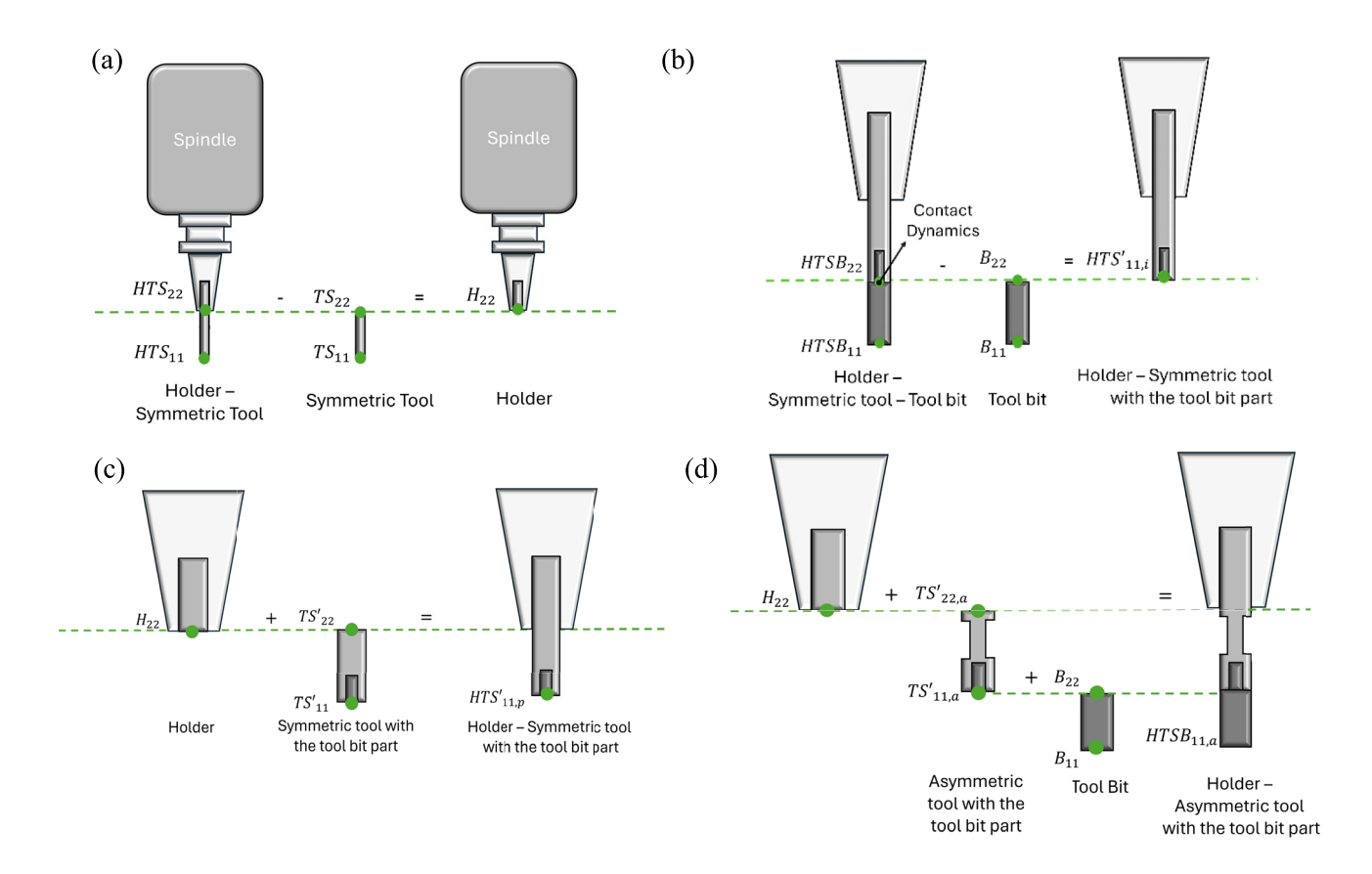


Fig. 2 The schematic illustration of the tool tip FRF prediction procedure: **a** Identification of the holder tip dynamics by inverse RCSA; **b** identification of the FRFs of the symmetric cutter shank tip with the tool bit inside by inverse RCSA; **c** prediction of the FRFs of the symmetric cutter shank tip with the tool bit inside by inverse RCSA; **c** prediction of the FRFs of the symmetric cutter shank tip with the tool bit inside by inverse RCSA; **c** prediction of the FRFs of the symmetric cutter shank tip with the tool bit inside by inverse RCSA; **c** prediction of the FRFs of the symmetric cutter shank tip with the tool bit inside by inverse RCSA; **c** prediction of the FRFs of the symmetric cutter shank tip with the tool bit inside by inverse RCSA; **c** prediction of the FRFs of the symmetric cutter shank tip with the tool bit inside by inverse RCSA; **c** prediction of the FRFs of the symmetric cutter shank tip with the tool bit inside by inverse RCSA; **c** prediction of the FRFs of the symmetric cutter shank tip with the tool bit inside by inverse RCSA; **c** prediction of the FRFs of the symmetric cutter shank tip with the tool bit inside by inverse RCSA; **c** prediction of the FRFs of the symmetric cutter shank tip with the tool bit inside by inverse RCSA; **c** prediction of the FRFs of the symmetric cutter shank tip with the tool bit inside by inverse RCSA; **c** prediction of the FRFs of the symmetric cutter shank tip with the tool bit inside by inverse RCSA; **c** prediction of the FRFs of the symmetric cutter shank tip with the tool by the symmetric cutter shank tip with the tool bit inside by inverse RCSA; **c** prediction of the FRFs of the symmetric cutter shank tip with the tool by the symmetric cutter shank tip with the symmetric cutter shank tip with the tool by the symmetric cutter shank tip with the tool by the symmetric cutter shank tip with the symmetric cutter

metric cutter shank with the tool bit inside by forward RCSA; **d** prediction of the tool tip FRF of the asymmetric tool by forward RCSA of the holder, asymmetric cutter shank and tool bit



identified by subtracting the predicted dynamics from the identified dynamics as shown in Eq. (23):

$$inv(K_{cp}) = HTS'_{11,i} - HTS'_{11,p}$$
 (23)

The tool tip FRF of the asymmetric cutter shank assembly is predicted as follows:

$$HTS'_{11,a} = \left[HTS'_{11,a}\right] - \left[HTS'_{12,a}\right] \cdot \left[\left[HTS'_{22,a}\right] + \left[H_{22}\right]\right]^{-1} \cdot \left[HTS'_{21,a}\right]$$
 (24)

$$HTSB_{11,a} = [B_{11}] - [B_{12}] \cdot [[B_{22}] + [HTS'_{11,a}] + [inv(K_{cp})]]^{-1} \cdot [B_{21}]$$
 (25)

where B_{11} , B_{12} and B_{22} are the analytically calculated tool bit FRFs, and $K_{\rm cp}$ is the contact parameter matrix at the interface of the symmetric cutter shank and the tool bit. It should be noted that all analytically calculated and predicted FRF terms contain both translational and rotational FRF components.

3 Validation of the predicted chatter stability

3.1 Experimental setup

The zero-order analytical (ZOA) method for predicting milling stability is used to study the effect of asymmetricity of the cutter. For this purpose, two identical four-tooth symmetric indexable end mills with 16 mm diameter are chosen. The cutter has two components: a shank with an internally threaded hole and an exchangeable milling head with a threaded section to fit into the shank. The cutter shank is Korloy MAT-M08-065-S16t [23], and the tool bit is Korloy AMM 1016HR-M08; both are made from steel. Insert type is Korloy APMT060208PDFR-MA with 0.8-mm corner radius. The cutter assembly is mounted inside

a BT40 shrink-fit type toolholder. Normally, the cutter has a symmetric geometry along its shank. As shown in Fig. 3, another asymmetric cutter was obtained by modifying the shank of a symmetric cutter. Two flat sections of 50-mm length were machined by wire electro-discharge machining, to reduce the thickness from 16 to 10 mm in one direction. Considering the 6 mm through hole within the cutter shank, 10-mm thickness would be acceptable with a web thickness of 2 mm; hence, this case provides the highest possible degree of asymmetricity for the fixed length of the flattened section. The clamping length of the cutter shank inside the holder was 46 mm.

Two impact hammer tests are conducted to identify the holder tip dynamics and the contact parameters at the cutter shank-tool bit interface. First, the holder-tool assembly was mounted into HAAS VF-2SS 3-axis milling machine which has a maximum spindle speed of 12,000 rpm. PCB 086C02 impact hammer with plastic tip, Dytran 3225F1 single-axis accelerometer, National Instruments NI9234 data acquisition module and CUTPRO [24] software were used to obtain FRFs and modal parameters of the cutter shank in Fig. 4a. Measuring the toolholder-cutter shank assembly by manual hammer was feasible because the measurement points had enough space in between, and the assembly was stiff enough that no double hitting issue was experienced. However, testing the toolholder-cutter shank-tool bit assembly by manual hammer was more prone to double hitting due to its high flexibility, and hitting at the same points was a concern due to the closely spaced measurement points on the tool bit. Therefore, the toolholder-cutter shank-tool bit assembly was tested by Maul-Theet vImpact-64 automatic hammer but with the same accelerometer and data acquisition module, as is shown in Fig. 4b. The sampling rate was 25,600 Hz, and the resolution was 1 Hz. Shure SM137 condenser microphone is used for measuring the sound during the cutting tests.

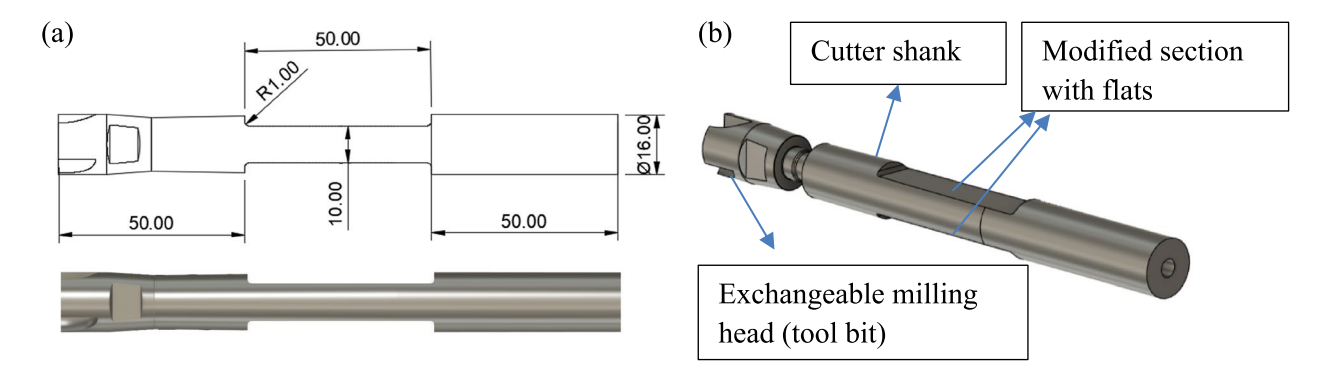
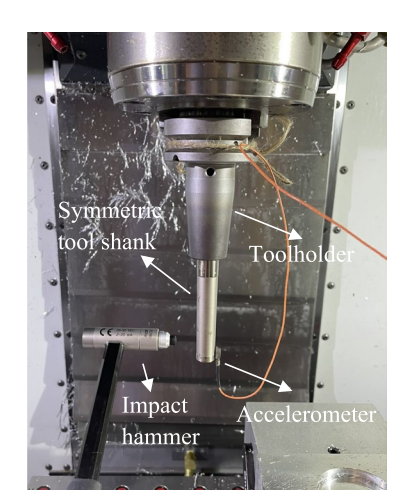


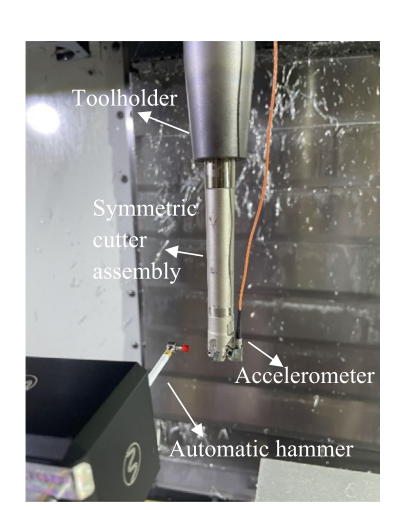
Fig. 3 Asymmetric indexable cutter with modified section on its shank (with originally 16 mm diameter) (a); and exploded view of the asymmetric indexable cutter assembly (b)



(a)

Fig. 4 Experimental setup for the symmetric cutter shank (a) and symmetric cutter shank with tool bit (b)





3.2 Identification of the dynamics with symmetric cutter

To identify the holder tip dynamics, impact hammer tests at the cutter shank tip (point 1) and at the connection point to the holder (point 2) are conducted with the symmetric cutter shank. Impact hammer test at the tip of the tool bit (point 1) and at the connection point to cutter shank (point 2) is conducted to identify the dynamics of the cutter shank with the parts of the tool bit inside. The FRF measurements are presented in Fig. 5.

The feed direction coincides with the y direction, while the normal direction is the x direction. The first vibration mode of the symmetric cutter shank (Fig. 5a) is measured around 1029 Hz and 1102 Hz in x and y directions, respectively, and the first mode of the symmetric cutter assembly (with shank and tool bit, as in Fig. 5b is

measured at 852 Hz and 859 Hz in x and y directions, respectively. The difference in damping ratio between the x and y directions would be expected due to the structural dynamics of the spindle-holder-tool system under the effect of spindle bearings and holder clamping mechanism being lumped at the tool tip. By applying inverse RCSA method, the dynamics at the holder tip and at the cutter shank-tool bit interface are identified. To obtain the contact parameters between the cutter shank tip and the tool bit, dynamics of the symmetric cutter shank tip with the part of the tool bit inside is predicted by forward RCSA method, and the contact parameters are obtained by employing Eq. (23). Next, the tool bit is coupled with the symmetric cutter shank by using Eq. (25), and the tool tip FRF of the symmetric cutter is predicted. The modal parameters for the symmetric cutter shank and the symmetric cutter are listed in Table 1.

(b)

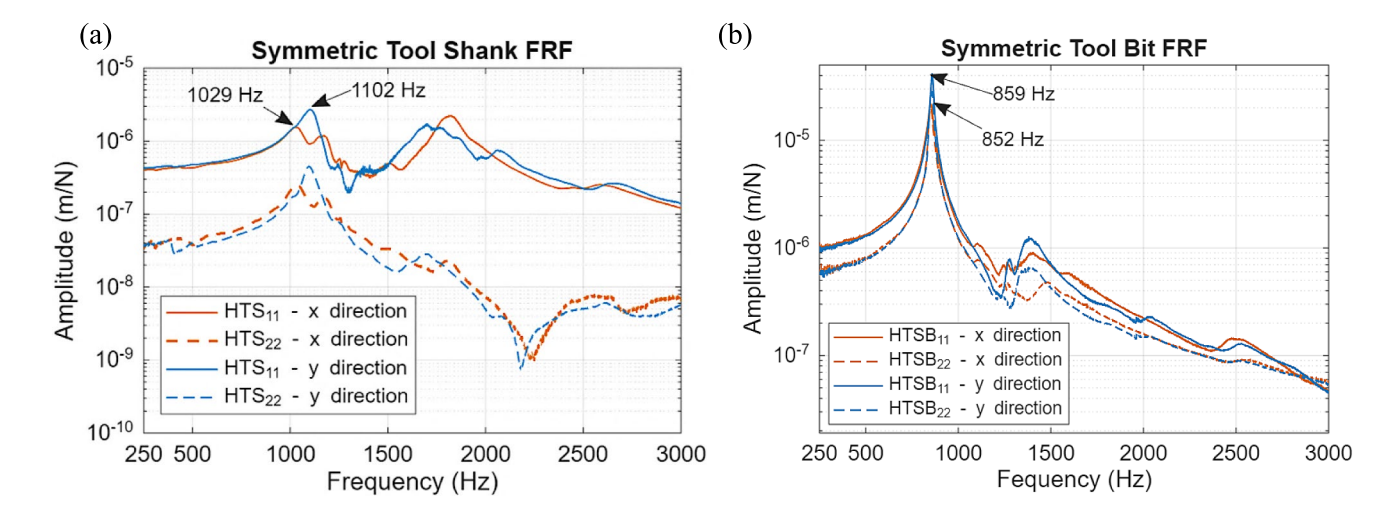


Fig. 5 FRFs of the symmetric cutter shank (a) and the symmetric cutter shank with the tool bit (b). Power spectra are given in the Appendix for the symmetric cutter shank in a and for the symmetric cutter shank with the tool bit in b



 -, where A_r is the modal constant **Table 1** The modal parameters of the symmetric cutter shank and the symmetric cutter assembly. $H(\omega) = \sum_{n=1}^{n} f(\omega)$

				-1=1 a	$-1 - 1 \omega_{n,r}^2 - \omega^2 + J \cdot 2\xi_r \omega_{n,r} \omega$			
	Symmetric cutter shank				Symmetric cutter assembly	ter assembly		
	Mode 1		Mode 2		Mode 1		Mode 2	
	x direction	y direction	x direction	y direction	x direction	y direction	x direction	y direction
Natural frequency (Hz)	1048	1108	1811	1701	852	859	1407	1418
Damping ratio (%)	3.58	3.25	3.06	4.35	1.64	0.76	3.34	2.01
Modal constant 3.87	3.87	8.37	17.42	16.47	20.37	18.21	3.61	3.15

3.3 Prediction of the dynamics of the asymmetric cutter

The tool tip dynamics of the asymmetric cutter is predicted for the case with the highest possible asymmetricity that is obtained by flattening a specified length along the cutter shank (as explained in Sect. 3.1). First, the holder tip dynamics identified by using the symmetric cutter shank is coupled with the asymmetric cutter shank of which dynamics calculated analytically by assuming it is formed by Timoshenko beams. Then, the tool bit receptance FRFs which are calculated analytically with the same method are coupled to the cutter shank by including the contact parameters obtained from the measurements of the symmetric cutter. Since the rotating coordinates of the cutter coincide interchangeably with the fixed x and y directions during the rotation, the modal parameters are averaged for u and v directions that are measured in x and y directions. The comparison of the predicted and measured modal parameters of the asymmetric cutter with the highest asymmetricity is given in Table 2, and FRF plots are given in Fig. 6. The natural frequency and modal stiffness values are predicted very well, so the location of the stability pockets is expected to be known accurately. The difference in the overpredicted damping ratio is due to the high damping ratio identified at the tip of cutter shank (see Table 1). However, the prediction error in the damping ratio would not be considered significant as the change in the stable depth of cut is not required for this study.

3.4 Experimental validation of the predicted chatter stability

Stability lobe diagrams (SLD) are predicted for both symmetric and asymmetric cutters, and they are experimentally validated by milling tests. Workpiece material was Al6082 alloy with the mechanistically identified cutting coefficients: $K_{\rm tc} = 774$ MPa and $K_{\rm rc} = 368$ MPa. The milling process was down milling with 75% radial immersion (i.e., $\phi_{st} = 60^{\circ}$; $\phi_{ex} = 180^{\circ}$) and 0.2 mm feed per tooth. For the cutter shank-tool bit interface, a torque wrench was used to keep the tightening torque controlled at 10.9 Nm. The radial runout of each of the four inserts on the cutter was measured in clockwise direction as 0, 44 µm, 26 μm, 48 μm, which were small compared to the feed rate. Moreover, the axial runout was measured as 12 µm, 0, 12 μm, 0, which were small compared to axial depth of cut. As can be seen in Fig. 7a, when directly measured FRFs used, simulated SLDs compared with the cutting test results show accurate predictions. When the predicted asymmetric cutter FRFs are used, the depth of cut is overpredicted due to the high damping ratio identified at the tip



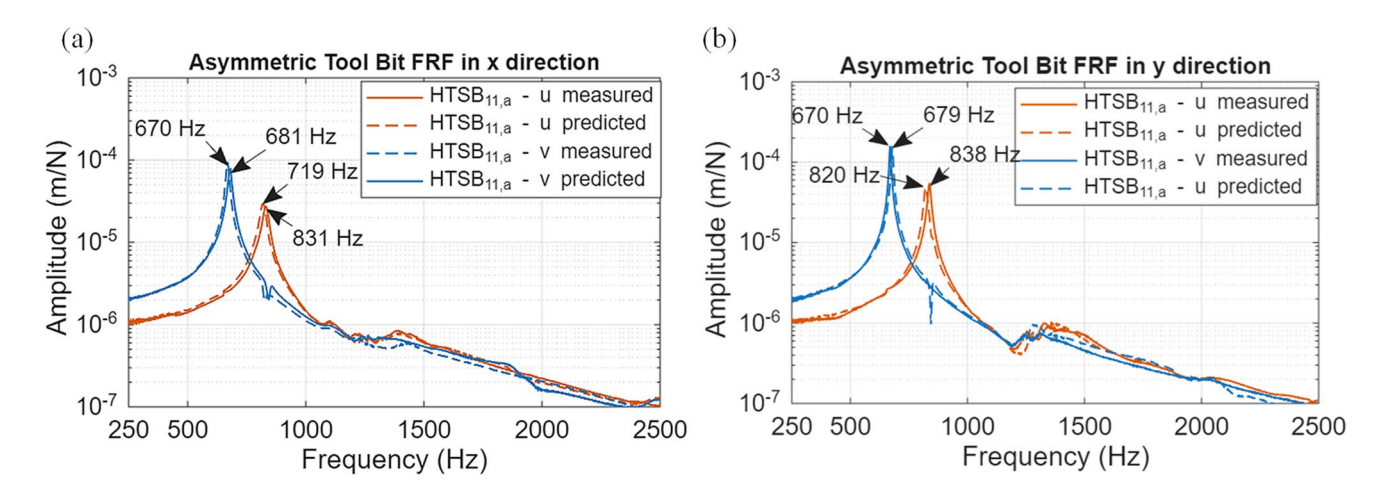


Fig. 6 Measured and predicted tool tip FRFs of the asymmetric cutter in x direction (a) and y direction (b). Power spectra for the hammer input are given in the Fig. 12c of the Appendix for the asymmetric cutter shank with tool bit in x and y directions

of the cutter shank as shown in Table 1. Since the cutter shank FRF measurements are used in the identification of the holder tip, it affects the predicted FRFs which are obtained by forward RCSA. However, the discontinuity in the chatter frequency diagram is captured well (Fig. 7b). During the tests, the surface marks and process sound signals were checked to decide on the chatter or stable condition. Sample machined surface images and FFT amplitude plots of the sound signals when machining with the asymmetric cutter are given in Figs. 8 and 9, respectively.

As can be seen in Fig. 7, the asymmetric cutter (with maximum material removed) cannot provide better stability due to the disappeared pocket at the high-speed machining region (i.e., $\Omega > 8000 {\rm rev/min}$). The chatter frequency diagram in Fig. 7b reveals that the disappearing pocket in the 12,000 rev/min > $\Omega > 10,000 {\rm rev/min}$) is due to the backward vibration mode (which is less than the original natural frequency at 655 Hz). On the other hand, the symmetric cutter's chatter frequency plot is continuous and decided by the forward vibration mode (which is higher than the original natural frequency ~830 Hz).

Table 2 Modal parameters of the asymmetric cutter in u and v directions

	Measured		Predicted		
	<i>u</i> direction	v direction	<i>u</i> direction	v direction	
Natural frequency (Hz)	834.5	669	820.5	679.5	
Damping ratio (%)	1.05	0.71	1.19	0.7	
Modal constant	20.88	28.13	22.73	26.63	

Hence, having the gyroscopic effects too high may cause a significant drop in stability due to the interactions between backward and forward vibration modes.

4 Discussion of the effect of the degree of asymmetricity

Section 3 demonstrated that the asymmetric cutter that is obtained by removing large material along the shank may cause a large reduction in stability which would not be acceptable. Knowing that the machine tool has a maximum spindle speed of 12,000 rev/min, it would be ideal to have the stability pocket's peak right below 12,000 rev/min. Moreover, the disappearing pocket is also observed when predicted FRFs are used, indicating that the accurate modal stiffness and natural frequency estimations are enough for knowing the limit of asymmetricity. Therefore, a balance between the shift and reduction of stability pockets can be sought based on the predicted FRFs.

To observe the effect of the asymmetricity degree, the tool tip FRFs of the asymmetric cutters with a = 1.5 mm, a = 2 mm and a = 2.5 mm (Fig. 10) are predicted, and modal parameters are listed in Table 3. SLDs are simulated for each condition with the given modal parameters by ZOA method as shown in Table 3.

As shown in Fig. 11a, the degree of asymmetricity affects the shift in the stability pocket at the maximum spindle speed region. Moreover, asymmetricity added by 5 mm material removal in ν direction moves the stability pocket's peak from 12,400 rpm (for the original symmetric cutter) to 11,700 rpm (i.e., to just below the maximum achievable



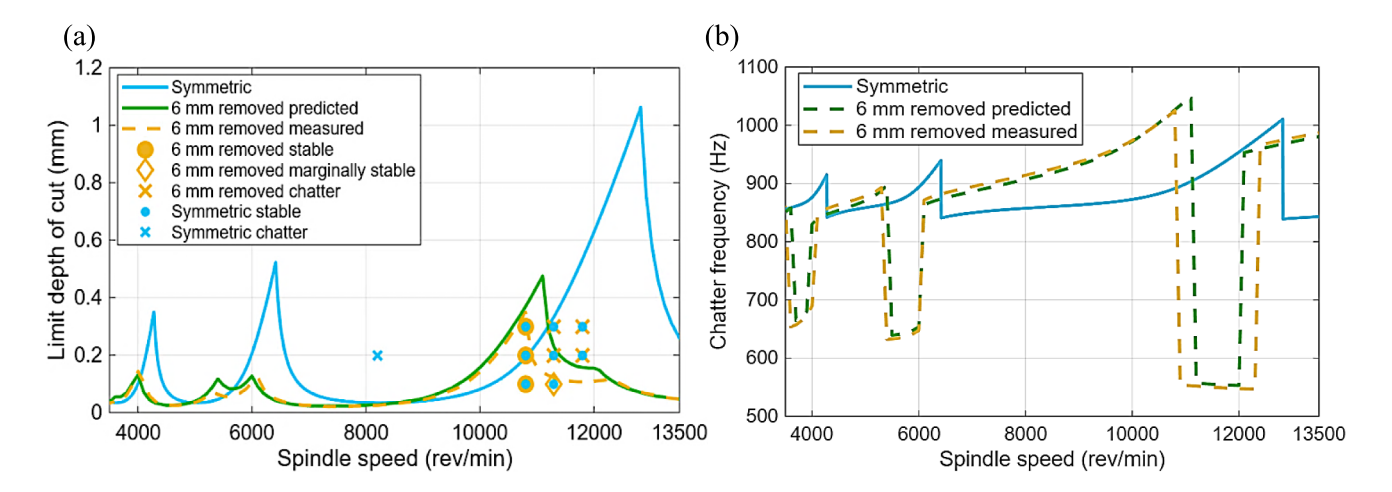


Fig. 7 Predicted SLD (a) and chatter frequency diagram (b) simulated by zero-order analytical (ZOA) method. Measured cutting test results are indicated by points on the SLD (a). Modal parameters for the symmetric and asymmetric cutter are given in Table 1 and

Table 2. Stable and unstable cutting processes were identified by visual evaluation of the machined surface and by the dominant vibration frequencies in the microphone signal

speed); therefore, it would perform better than other cases in Fig. 11. On the other hand, although it experiences a significant drop around 12,000 rev/min, the asymmetric cutter with 6 mm removed may also be preferred as its stability pocket appears at 10,800 rev/min.

5 Conclusion

A modeling procedure based on RCSA was proposed to identify a sufficient degree of cutter asymmetry (or, non-axisymmetry) to move the location of the stability pocket under the maximum spindle speed of the machine tool. Moreover, the type of indexable end mill with an exchangeable head (or, tool bit) was used for the first time in this study. The independence between the tool bit's mass and shank's stiffness of such cutters would give many design opportunities to tune the natural frequencies. In this study, the shank side was modified to create an non-axisymmetric cross sectional geometry that leads to distinct natural frequencies along two rotating coordinate directions of the cutter. The effects of each degree of asymmetry on the tool tip FRF were predicted by forward RCSA methodology, which used the lumped dynamics and contact parameter matrices

that were identified by inverse RCSA using the original symmetric cutter assembly. The milling experiments validated the prediction that the stability pocket would be disappeared when a cutter with the highest degree of asymmetricity was used. Therefore, a suitable degree of asymmetricity may be designed to keep the stability pocket under the maximum spindle speed of the machine tool.

This study focused on non-axisymmetric cutters' potential in terms of machining dynamics, making them a consideration for future tool design aspects. While the inaccuracies in identifying the damping ratio through inverse RCSA introduced prediction errors for stable depth of cut limit, the stability pocket locations for the aymmetric cutter were estimated well due to the accuracy in predicting the modal mass and stiffness parameters at the tool tip. However, the accuracy of the damping ratio identification may still need improvement to study the balance between dynamic performance and static rigidity, which is another concern for long end mills.

The method may be developed further in the future considering the following:

 For the repeatable identification of the toolholder-cutter shank interface, the cutter shanks were always kept inside the holders through the experiments. Therefore,



Fig. 8 Pictures of the surfaces after machining 0.2-mm depth of cut at three spindle speeds: 10,800 rev/min, stable (a), at 11,300 rev/min, chatter (b), and at 11,800 rev/min, chatter (c)



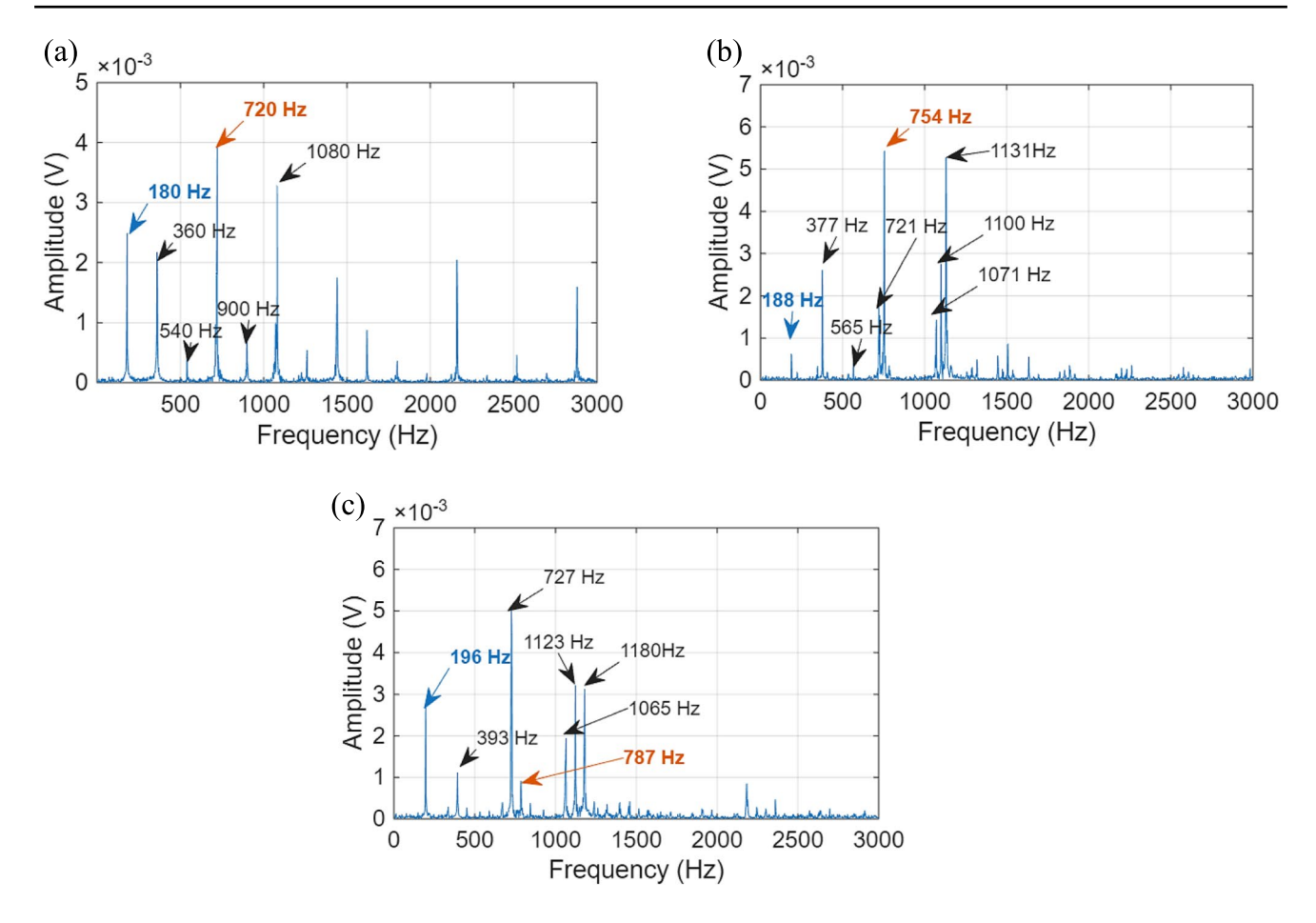


Fig. 9 FFT amplitude plots of the sound signals gathered when milling at 0.2-mm depth of cut with the asymmetric cutter: **a** stable cutting at 10,800 rev/min; **b** chatter at 11,300 rev/min; **c** chatter at

11,800 rev/min. The spindle rotation frequencies and tooth passing frequencies are labeled blue and orange, respectively, to identify the chatter frequencies easily

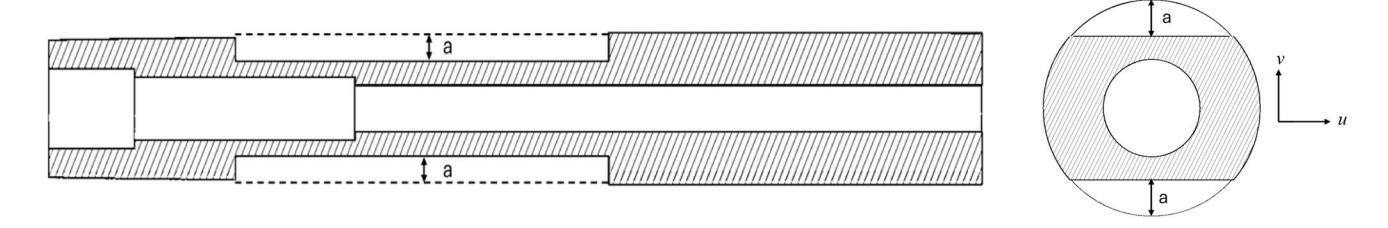


Fig. 10 Cross-sectional view of the asymmetric cutter

Table 3 Modal parameters of the asymmetric cutter with 3 mm, 4 mm and 5 mm reduction (indicated by *a* in Fig. 10) in total diameter

	3 mm		4 mm		5 mm	
	u direction	v direction	u direction	v direction	<i>u</i> direction	v direction
Natural frequency (Hz)	827.5	791.5	827	765	824.5	728
Damping ratio (%)	1.33	1.23	1.30	0.91	1.30	0.89
Modal constant	22.37	26.01	22.42	25.09	23.58	29.81



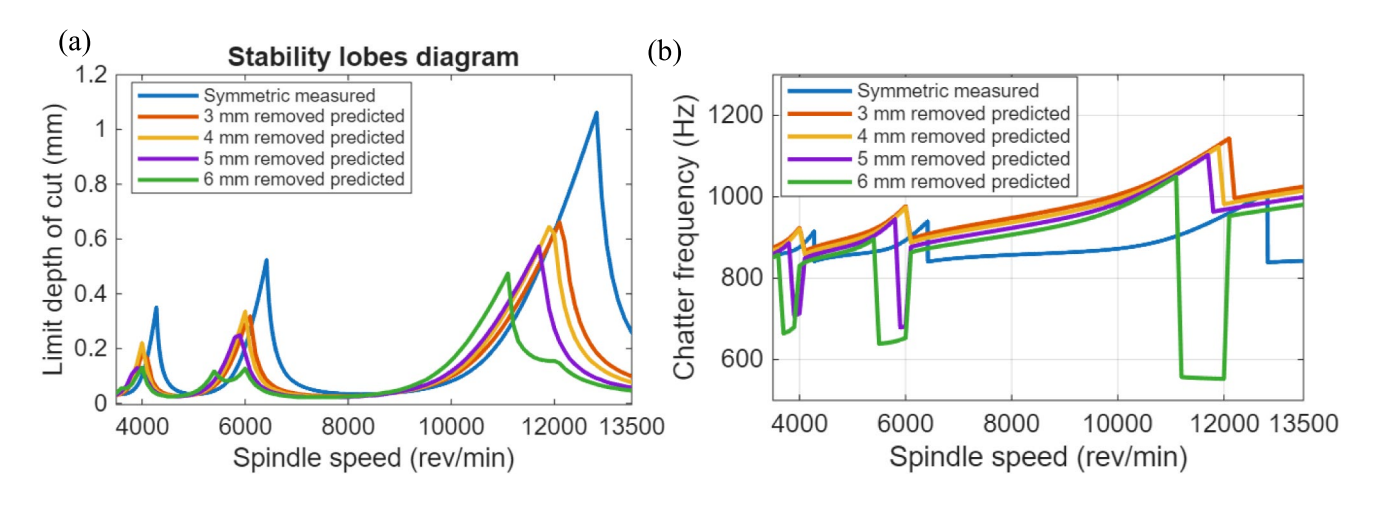


Fig. 11 Simulated SLDs (a) and chatter frequency diagrams (b) for various degrees of asymmetricity. Modal parameters for the symmetric cutter are given in Table 1, and the asymmetric cutters are given in Table 2 and Table 3

two different tool holders were used, with one of them having the symmetric shank, and another with the asymmetric shank. Although the positioning differences of the cutter shank inside toolholder may vary from one assembly to another, predicted tool tip FRF has acceptable accuracy. However, the effect of the toolholder clamping position would be an interesting aspect to investigate in the future.

The purpose of the study was to reduce the effort to identify the contact stiffness and damping by long testing

procedures. Thus, the dynamics at the toolholder–cutter shank was not identified explicitly, i.e., the predicted FRF at the contact includes the spindle's lumped dynamics at the contact and the contact stiffness and damping. Although the stiffness and damping parameters at the cutter shank—tool bit interface were identified, they are calculated at each frequency value and a single set of contact stiffness and damping parameters was not obtained. Hence the modeling of the contact may need more detailed analysis in the future.



Appendix

The power spectral density (PSD) of the hammer impulse for symmetric tool shank and symmetric tool bit measurements are given in Fig. 12.

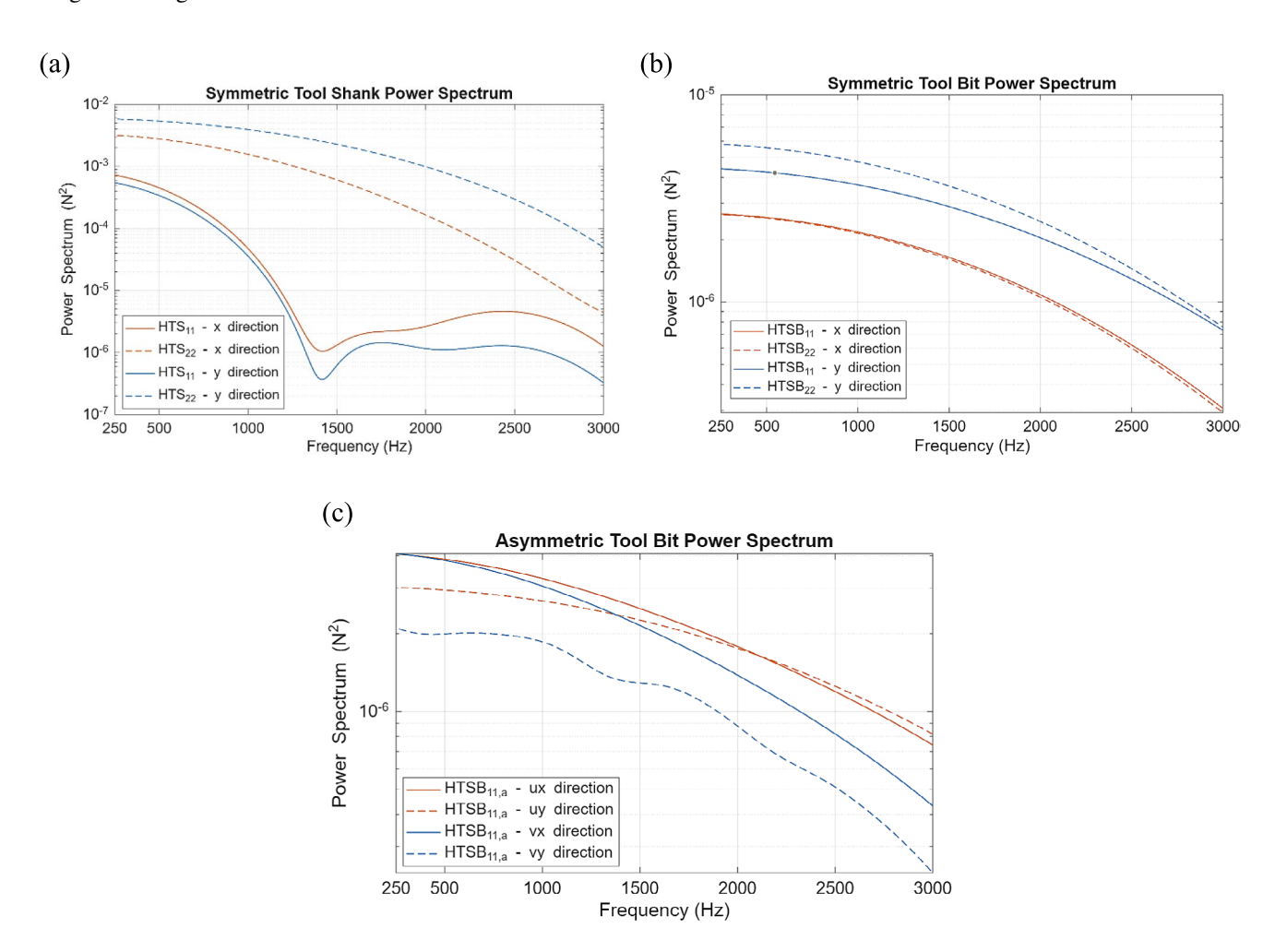


Fig. 12 Power spectra of the hammer impulse for the FRF measurements of: symmetric tool shank (a); symmetric tool bit (b) and asymmetric tool bit (c)

Acknowledgements The authors would like to thank the UoM/FSE's Nancy Rothwell Building mechanical workshop team and Dr Ramazan Hakki Namlu (Atilim University) for their support during the experiments.

Funding The first author is funded by the University of Manchester's (UoM) Department of Mechanical, Aerospace and Civil Engineering's Exceptional Women in Engineering PhD Scholarship. Corresponding author acknowledges the partial supports of the Engineering and Physical Sciences Research Council's Innovation Launchpad Network + Researcher in Residence scheme [grant numbers EP/W037009/1, EP/X528493/1] and School of Engineering Pump Priming, Theme Development and Dissemination fund.

Department of Mechanical, Aerospace and Civil Engineering, University of Manchester, Exceptional Women in Engineering PhD Scholarship, Hatice Elif Tola Demirel, Engineering and Physical Sciences Research Council, EP/W037009/1, Z. Murat Kilic, EP/X528493/1, Z. Murat Kilic, School of Engineering, University of Manchester, Pump Priming, Z. Murat Kilic, Theme Development, Z. Murat Kilic, Dissemination fund, Z. Murat Kilic

Declarations

Conflict of interest The authors declare no competing interests.

Open Access This article is licensed under a Creative Commons Attribution 4.0 International License, which permits use, sharing, adaptation, distribution and reproduction in any medium or format, as long as you give appropriate credit to the original author(s) and the source, provide a link to the Creative Commons licence, and indicate if changes were made. The images or other third party material in this article are included in the article's Creative Commons licence, unless indicated



otherwise in a credit line to the material. If material is not included in the article's Creative Commons licence and your intended use is not permitted by statutory regulation or exceeds the permitted use, you will need to obtain permission directly from the copyright holder. To view a copy of this licence, visit http://creativecommons.org/licenses/by/4.0/.

References

- Altintas Y, Stepan G, Budak E, Schmitz T, Kilic ZM (2020) Chatter stability of machining operations. J Manuf Sci Eng 142:110801. https://doi.org/10.1115/1.4047391
- Tobias S, Fishwick W (1958) Theory of regenerative machine tool chatter. The Engineer (London) 205:199–203
- Tlusty J, Polacek M (1963). The Stability of the Machine Tool Against Self Excited Vibration in Machining. In: Proceedings of the ASME International Research in Production Engineering, Pittsburgh, PA, pp 465–474
- 4. Altintas Y, Budak E (1995) Analytical prediction of stability lobes in milling. CIRP Ann Manuf Technol 44:357–362
- Insperger T, Stépán G (2002) Semi-discretization method for delayed systems. Int J Numer Methods Eng 55:503–518. https:// doi.org/10.1002/nme.505
- Munoa J, Beudaert X, Dombovari Z, Altintas Y, Budak E, Brecher C, Stepan G (2016) Chatter suppression techniques in metal cutting. CIRP Ann Manuf Technol 65:785–808. https://doi.org/10. 1016/J.CIRP.2016.06.004
- Mativenga P, Schoop J, Jawahir IS, Biermann D, Kipp M, Kilic ZM, Özel T, Wertheim R, Arrazola P, Boing D (2024) Engineered design of cutting tool material, geometry, and coating for optimal performance and customized applications: a review. CIRP J Manuf Sci Technol 52:212–228. https://doi.org/10.1016/j.cirpj. 2024.06.001
- van Zyl D, Altintas Y, Ostling D (2022) Parametric design of boring bars with adaptive tuned mass dampers. CIRP J Manuf Sci Technol 38:491–499. https://doi.org/10.1016/j.cirpj.2022.06.003
- Yang Y, Yang Y, Liu H-C, Wan M, Zhang W-H (2024) A new cutting tool filled with metallic lattice and design method for vibration suppression in milling. Mech Syst Signal Process 212:111310. https://doi.org/10.1016/j.ymssp.2024.111310
- Astarloa A, Comak A, Mancisidor I, Fernandes MH, Munoa J, Dombovari Z (2022) Improvement of boring operations by means of mode coupling effect. CIRP J Manuf Sci Technol 37:633–644. https://doi.org/10.1016/j.cirpj.2022.03.008
- Mohammadi Y, Azvar M, Budak E (2018) Suppressing vibration modes of spindle-holder-tool assembly through FRF modification for enhanced chatter stability. CIRP Ann 67:397–400. https://doi. org/10.1016/j.cirp.2018.03.003

- Ren Y-Y, Wan M, Zhang W-H, Yang Y (2023) A review on methods for obtaining dynamical property parameters of machining processes. Mech Syst Signal Process 194:110280. https://doi.org/10.1016/j.ymssp.2023.110280
- Bediz B, Arda Gozen B, Korkmaz E, Burak Ozdoganlar O (2014)
 Dynamics of ultra-high-speed (UHS) spindles used for micromachining. Int J Mach Tools Manuf 87:27–38. https://doi.org/10.1016/j.ijmachtools.2014.07.007
- Cheng CH, Schmitz TL, Duncan GS (2007) Rotating tool point frequency response prediction using RCSA. Mach Sci Technol 11:433–446. https://doi.org/10.1080/10910340701539866
- Li C-J, Ulsoy AG, Endres WJ (2003) The effect of flexible-tool rotation on regenerative instability in machining. J Manuf Sci Eng 125:39. https://doi.org/10.1115/1.1536657
- Eynian M, Altintas Y (2010) Analytical chatter stability of milling with rotating cutter dynamics at process damping speeds. J Manuf Sci Eng 132:021012. https://doi.org/10.1115/1.4001251
- Comak A, Ozsahin O, Altintas Y (2016) Stability of milling operations with asymmetric cutter dynamics in rotating coordinates.
 J Manuf Sci Eng, Transactions of the ASME 138. https://doi.org/ 10.1115/1.4032585
- Baumann J, Wirtz A, Siebrecht T, Biermann D (2020) Disturbance of the regenerative effect by use of milling tools modified with asymmetric dynamic properties. J Manuf Mater Process 4:67. https://doi.org/10.3390/jmmp4030067
- Kilic ZM, Altintas Y (2012) Stability of peripheral milling operations with long end mills. In: Procedia CIRP pp 103–108. https:// doi.org/10.1016/j.procir.2012.10.019
- Park SS, Altintas Y, Movahhedy M (2003) Receptance coupling for end mills. Int J Mach Tools Manuf 43:889–896. https://doi. org/10.1016/S0890-6955(03)00088-9
- Namazi M, Altintas Y, Abe T, Rajapakse N (2007) Modeling and identification of tool holder–spindle interface dynamics. Int J Mach Tools Manuf 47:1333–1341. https://doi.org/10.1016/J. IJMACHTOOLS.2006.08.003
- Ozguven HN (1990) Structural modifications using frequency response functions. Mech Syst Signal Process 4:53–63
- Korloy MAT-M08–065-S16T Modules cylindrical shank -Screw mounting - ToolsUnited, (n.d.). https://toolsunited.com/EN/ Article/Details/24696400130752321 Accessed 23 Jan 2025
- 24. CUTPRO (2021) https://www.malinc.com Accessed 24 Jan 2025

Publisher's Note Springer Nature remains neutral with regard to jurisdictional claims in published maps and institutional affiliations.

